MATERIALS SCIENCE

Single-chirality nanotube synthesis by guided evolutionary selection

Boris I. Yakobson[1,2]* and Ksenia V. Bets[1]

Bringing to fruition the tantalizing properties, foreseen since the discovery of carbon nanotubes, has been hindered by the challenge to produce a desired helical symmetry type, single chirality. Despite progress in post-synthesis separation or somewhat sporadic success in selective growth, obtaining one chiral type at will remains elusive. The kinetics analysis here shows how a local yet moving reaction zone (the gas feedstock or elevated temperature) can entice the tubes to follow, so that, remotely akin to proverbial Lamarck giraffes, only the fastest survive. Reversing the reaction to dissolution would further eliminate the too fast-reactive types so that a desired chirality is singled out in production.

INTRODUCTION

Among the low-dimensional materials, carbon nanotubes (CNTs) have been an iconic example: the ~1-nm-thin hollow cylinders emerged (*1*) as unexpectedly stable, strong molecular structures with helical symmetry, helicity (*2*), often expressed by chiral angle, $0 < \chi < 30°$ or a pair of chiral indexes (n,m) (*3*). Apart from the topmost mechanical strength in composites or fibers (*4*, *5*), all CNTs' finer properties—electronic, optical, sensing—depend greatly on the chirality, χ. That is why the nonspecific syntheses, where the tubes of different χ types are produced intermixed together, have been thwarting a plethora of tantalizing applications (*6*). Over the years, this motivated remarkable progress in postsynthetic-type separation based on the use of discriminating surfactants, including success with DNA strands, and isopycnic centrifugation (*7*–*9*). Concurrent approaches to achieve selectivity directly in synthesis, either at CNT nucleation or combining nucleation and growth (*10*–*12*), yielded sometimes remarkable but not yet broadly reproduced results. Despite all these important efforts, no method has been found or even proposed to produce nanotubes of the "right," prechosen chirality; this "holy grail" (*13*) has remained elusive for decades.

Below, we present a strategy that enables the selective synthesis of nanotubes based on their growth speed and, in principle, would allow the production of single-chirality CNT. Moreover, if followed by a dissolution process, reverse to the growth (such as etching with appropriate reactant), then one can achieve the growth of single chosen chirality. The method is based on recognizing an intrinsic functional relationship between the growth speed of each CNT type and its chirality: At given conditions, some grow faster while others grow slower, as defined by the reaction rate constants for each, $\chi \rightarrow k(\chi) \equiv k_\chi$. Second, one has to have the reaction zone (say, feedstock supply) not uniform but localized. The third and important is for the reaction zone not to stay still but to steadily move ahead so that its speed V determines whether all the CNTs can keep up or only the faster species survive and grow while the slower ones fall behind and perish. This creates a simple yet powerful guided evolutionary selection: By the choice of the zone propagation speed, one relies on process kinetics to separate the CNT ensemble by the rate constants k_χ and, therefore, the underlying helicities, χ. Note that in this paragraph and in the following, χ is mostly used as a formal label identifier, which may include both chiral angle and diameter or, equivalently, the index pair (n,m).

RESULTS

The carbon feedstock atmosphere (e.g., CH_4 and C_2H_2) of some concentration c, catalyst particles (typically, a metal), and elevated temperature T, are preeminent conditions for the growth of all types of CNT. However, the growth speeds v_χ and, consequently, lengths l_χ [both are ensemble or time averaged, as $<v(t)>_{\chi=\text{const}}$] do depend on helicity: $v_\chi = k_\chi \cdot c$ and $l_\chi = v_\chi \cdot t$. It is observed in experiments (*14*) and theory (*15*, *16*) that nanotubes of different helicity display distinctly different growth speeds, roughly because helicity, by virtue of the sheer geometry of the tube, dictates the number of kinks at its edge (Fig. 1A, inset), where C_2 dimers land and readily bind (*1*, *15*).

Although the growth speed and the integral length of each tube are direct functions of its helicity, the absolute positions of the tube active tips differ across the various synthesis approaches. In the gas-phase chemical vapor deposition (CVD) reactors, the tubes' locations are randomized by carrier gas, often turbulent (*12*, *17*). In very common root growth of carpets or forest CVD, the active ends are attached to catalysts affixed to the substrate, fully static (*18*–*20*).

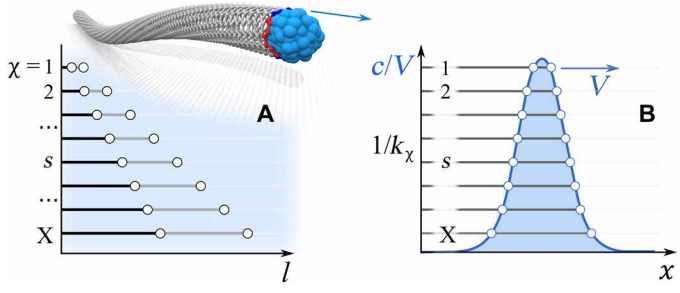

Fig. 1. Uniform versus localized feedstock gas distribution. (**A**) Nanotubes of helicities $\chi = 1, 2, \ldots,$ X, shown ordered by growth constants k_χ in uniform atmosphere attain the lengths in proportion to k_χ, as shown; top inset illustrates the kite growth (*21*–*28*) with the tube tip–catalyst moving freely as it grows. (**B**) Localized feedstock concentration $c(x)$, shaded blue, moves at speed V, while different CNTs achieve steady-state positions according to the k_χ values; the selected one is marked s.

[1]Department of Materials Science and NanoEngineering, Rice University, Houston, TX 77005, USA. [2]Department of Chemistry, Rice University, Houston, TX 77005, USA. *Corresponding author. Email: biy@rice.edu

The most relevant approach here is where the catalysts detach from the substrate so that the active tube tip floats freely with a laminar gas flow, constrained solely by the length of the tube tail, resting on the substrate (Fig. 1A, inset); aptly dubbed the "kite mechanism" in early works (*21*, *22*), it developed quite efficiently to grow ultralong CNT (*23*–*28*). In the kite setup, the tips of the growing CNT will spread in space systematically, the faster getting ahead of the slow, akin to wave dispersion of sound or light, whose speed is a function of wavelength or frequency. In a uniform atmosphere, such dispersion will vary the lengths of CNT, unremarkably per se.

Illustrated in Fig. 1A, the tubes are ordered top-down by ascending k_χ values and numbered $\chi = 1, 2, \ldots, X$ but, in reality, grow intermixed, obscuring any systematic length differences. The intrinsic difference in growth speeds among the helicities cannot offer chiral selectivity: The evolutionary selection process recognized early for the domains of growing polycrystal (*29*) is not operational for the CNTs, which grow independently and not compete. Key ideas come when considering the feedstock supply not uniform, as in a typical CVD chamber, but local, of concentration $c(x)$ of maximum c_0 and vanishing to peripheries, $|x| > w$ [e.g., realized by a nozzle for graphene (*30*), where the local feed served to prevent unwanted secondary nucleation]. This must "entice" the tubes to reach the location rich in feedstock. The situation resembles (remotely, for obvious lack of the hereditary aspect here) the proverbial, from pre-Darwinian theories, Lamarck giraffes stretching their necks to reach the juicier tree crowns. If the feedstock-rich (or elevated T) reaction zone moves slowly at speed V, different tubes reach concentration levels where they can grow in sync, according to $k_\chi \cdot c(x - Vt) = V$ at the steady state. In a reference frame moving along with the reaction zone, a more convenient form is

$$1/k_\chi = c(x_\chi)/V \tag{1}$$

as plotted in Fig. 1B, along with the root solutions.

Although the distributed k_χ values again result in a spatial dispersion (growing tip positions x_χ spread along the slopes of the reaction zone), overall, the CNTs extend at common speed V; the localized zone seems to even suppress the selectivity in χ, compared to uniform atmosphere case, $c(x)$= const (Fig. 1A). [We do not discuss the growth termination because a number of studies suggest the possibility of growing CNT uninterrupted without length limitation (*23*).]

The growth of an individual tube is inherently stochastic, with feedstock molecules decomposed on the catalyst particle, providing the carbon to the tube edge. Inevitably, its elongation, speed, and the tip position fluctuate by δx [as seen in experiments (*31*)]. Even more notable must be the variations in the gas concentration $\delta c(x)$ or the temperature $\delta T(x)$. It is important therefore to pay attention to the stability of those solutions in Fig. 1B, with respect to such basic perturbations, orthogonal in the c-x plane (Fig. 2). First, if the tube length fluctuates, then its tip position shifts by $\delta x = \delta l$ from the stationary point of Eq. 1; accordingly, the feed concentration changes by $(\partial c/\partial x)\cdot\delta x$ and the growth speed will also change by $d\delta x/dt = k(\partial c/\partial x)\delta x$. Perturbative evolution $\delta x(t) = \delta x \cdot e^{k(\partial c/\partial x)t}$ is exponentially amplified or damped, defined by the positive or negative slope $(\partial c/\partial x)$ of the concentration curve. This Lyapunov exponential stability is shown in Fig. 2A by the arrow trajectories, on the right slope returning to the stationary point (stable growth), while, on the left, the trajectories abandon the unstable solution, that is,

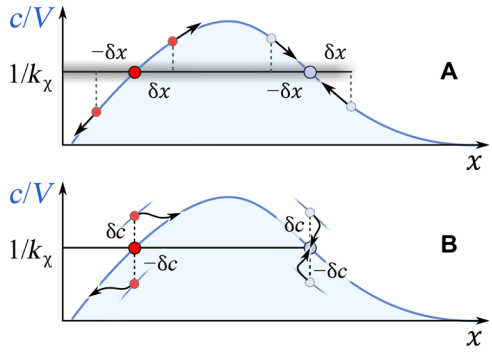

Fig. 2. Stability analysis of the CNT growth dynamics. The gas supply distribution $c(x - Vt)$, advancing with a speed V, in a reference frame moving along with the reaction zone $c(x)$ is fixed. (**A**) Fluctuations of CNT length $\pm\,\delta x$ cause instability near the red stationary point, but it is stable near the hollow circle on the right; small arrows point in the relaxation directions. The blurred width of the horizontal line k_χ = const represents possible speed fluctuations. (**B**) Fluctuations of gas concentration $\delta c(x)$ develop instability near the red stationary point, but growth is stable on the right slope; arrows show the relaxation trajectories.

the tube either falls behind the moving reaction zone or accelerates to bypass the zone peak and reach the stable stationary point on the right front slope. For a single CNT, its growth rate constant can also fluctuate because of changes in the edge geometry (or catalyst particle structure) (*32*), as marked by the blurred width of the $1/k$-horizontal line in Fig. 2A. We find that a variation δk causes the CNT tip to depart from the stationary point, $\delta x = (\delta k/k)c(\partial c/\partial x)^{-1}(e^{k(\partial c/\partial x)t} - 1)$, again diverging on the left $(\partial c/\partial x > 0)$ but stable on the right slope $(\partial c/\partial x < 0)$ of the reaction zone.

More substantial can be gas concentration variation $\delta c(x)$, corresponding to a vertical shift in Fig. 2B. Again, for a tube tip at x, it means that speed change by $\delta v = k\delta c(x)$ and, past time increment dt, an additional displacement $dx = k\delta c(x)dt$ will change the local feed concentration by $d\delta c = (\partial c/\partial x)dx = k(\partial c/\partial x)\delta c(x)dt$. Thus, one has $d/dt\ \delta c = k(\partial c/\partial x)\delta c$, meaning the disturbance evolves as $\delta c(t) = \delta c \cdot e^{k(\partial c/\partial x)t}$, repeating the same rule as for δl and δk fluctuations: unstable on the left slope of $c(x)$, where $\partial c/\partial x > 0$, and stable on the right, at $\partial c/\partial x < 0$.

With such two branches of solutions, unstable at the back and stable in front of moving feedstock, if the reaction zone (a gas nozzle or a heated spot) moves at low speed V, then the ensemble of growing tubes overall follows, their tips tracking the stable roots x_χ of the Eq. 1, on the front of $c(x)$. Limited spatial spread of all x_χ, however, offers no way to single out a selected $\chi = s$.

The situation changes drastically if the reaction zone moves faster, at $V > c_o \cdot k_1$. The steady-state solutions of Eq. 1 cease to exist for the slower types, which "slide down" the left slope of $c(x)$ and stop at the no-gas, no-reaction positions [reaching trivial solutions $v_\chi = 0$, $c(x_\chi) = 0$], while the faster types continue to grow at speed V (Fig. 3A). This bifurcation is central to kinetic selection, as it splits the CNT ensemble into two sets, by helicity, slow $1 < \chi < s$ and fast $s \le \chi < X$, with only the latter being produced in large amounts while the former are selected out. In a particular case of high-speed $V_{max} \approx c_o k_X$, only one fastest type $\chi = X$ can keep up (right peak in Fig. 3A). Such carefully tuned zone speed would allow the growth of a single chiral type, having the long-standing problem solved, however, solved not quite fully.

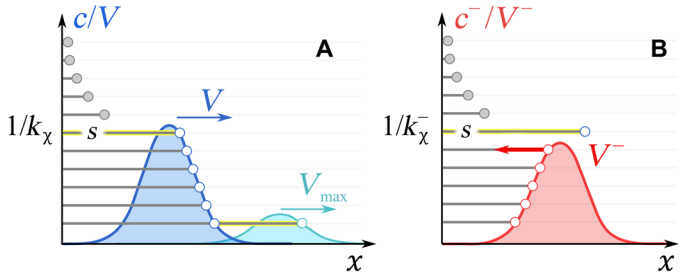

Fig. 3. Chiral selection mechanism. (**A**) With the reaction zone moving faster, for the slow CNTs of $\chi = 1$ to $(s-1)$, above the $c(x)$ peak, Eq. 1 has no roots, and the CNT ensemble bifurcates into surviving and growing $\chi = s$ to X and other $\chi < s$ perishing. Highest V_{max} selects only one chirality type $\chi = X$. (**B**) In the reversed process (etching, gasification) the reaction zone, shown as a red peak moving left, will eliminate all types $\chi > s$, leaving only selected helicity $\chi = s$ intact.

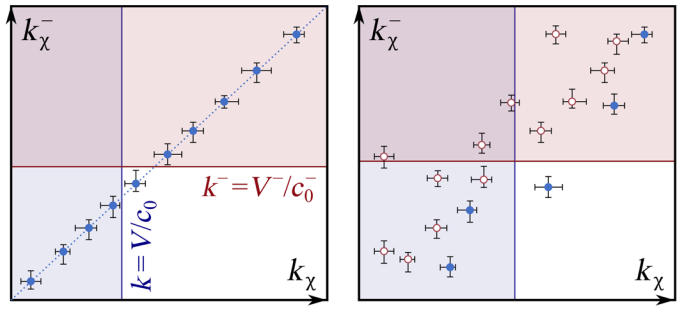

Fig. 4. The selection possibility maps. (**Left**) If $k^-_\chi \propto k_\chi$ (a condition warranted near-equilibrium or for model mechanisms), then any chirality from the set can be selectively synthesized in grow-and-reduce cycle. Selection growth eliminates all slower species ($k_\chi < V/c_0$, shaded blue); the etching dissolves all the "too reactive" types ($k^-_\chi > V^-/c_0^-$, shaded red). (**Right**) If condition $k^-_\chi \propto k_\chi$ does not hold, then still some chiralities can be selectively produced by being canvassed into the white rectangle, a clear possibility for some (solid blue), although not all (red circles) chiral types.

While such guided growth at near-top speed $c_0 k_X$ does yield a single chirality, it is not arbitrarily chosen. Could one particular $\chi = s$ be selected from the whole spectrum $1 \le s \le X$ and the process planned to produce solely s type? For s with a generic midrange rate constant k_s, the above describes how to eliminate all too slow $k_\chi < k_s$ and preserve all sufficiently fast-growing CNT, setting the lower bound on the constants, $k_s \le k_\chi$, not a single but several types. How can an upper bound be imposed to further eliminate species of rate constants above the k_s, reacting faster?

The ability of CNT to either grow by streaming out of the catalyst particle or be dissolved in it and shorten [e.g., reversed by the current direction (*33*)] suggests invoking such reversal while also relying on detailed balance in chemistry. In the generic growth reaction, CNT_l + "CH" $\leftarrow^{k^-,\,k} \rightarrow CNT_{l+1} + H_2$, the feedstock, often a hydrocarbon CH, adds C atoms to increase length l (growth constant k) or can also be reversed to etching/gasification (rate constant k^-), as observed in experiments by changing gas conditions (*34*–*36*). In equilibrium, the reaction rates forward and back must be the same for all χ: $k_\chi\, c_{eq} = k^-_\chi\, c^-_{eq}$ (c^- is the concentration of "etchant," e.g., H_2 above). That is, $k_1/k_1^- = k_2/k_2^- = \ldots = (c/c^-)_{eq} = \text{const}$, invariant across all χ types. Away from equilibrium, if a certain tube grows fastest (at elevated c), then it must also shrink faster than all others (if c^- is in excess). It is helpful to our approach in a way that the ranking of types by k^-_χ values in Fig. 3B remains the same as was the ranking by k_χ in Fig. 3A (also seen in Fig. 4A). That is, if the gas in the reaction zone changes so that growth is reversed to etching/gasification, then the latter should eliminate the fast-etched species, establishing an upper bound on surviving types, by k^-_χ values. At proper conditions (the ratio c_o^-/V^-), one can narrow the choice to just one type to be selected, s. Figure 3 illustrates the above: The guided-selection growth already produced an ensemble of all helicities with $k_\chi \ge k_s$ (Fig. 3A); therefore, the reverse process of decay/etching can be set for a peak concentration c_o^- moving at speed $V^- = (k^-_s + \Delta k)c_o^-$, slightly too fast for dissolving the s type, whose highest etching speed is only $k_s^- c_o^-$. The smallness of Δk ensures full dissolution of all others, with $k^-_\chi > k_s^-$ (lines below the peak height in Fig. 3B), while its positive value $\Delta k > 0$ makes certain that the type s remains preserved.

Nevertheless, the selected type s is also temporarily exposed to etchant in this reverse process, and the loss of its material (length) can be estimated (this paragraph refers to the selected "s" and reversed reaction/etching "–" but, for brevity, omits these indices). A Gaussian peak concentration $c(x)$, of height c_o and width w, near its maximum, is $c(x)/c_o \approx 1 - (x/w)^2$. First, from the peak-top (moving at speed V), the CNT tip falls behind at speed $\Delta k c_o$. Near the peak, this CNT tip trailing due to Δk dominates the factor of concentration decrease, $\Delta k > k(x/w)^2$. Then, having $x \approx \Delta k c_o t$ allows one to estimate the tip residence time in the reactive zone, $t = w/[c_o(k\Delta k)^{1/2}]$. The portion of tube length lost (etched) during this time is $\Delta l \sim Vt = w(k/\Delta k)^{1/2}$. In reality, for a typical diameter range, the whole spectrum of $\{k_\chi\}$ amounts to 30 to 40 spaced values so that roughly $k/\Delta k \sim 30$ to 40, and thus, this loss of length is an order of a few widths of the reaction zone w. The latter can be kept rather limited or even negligible in comparison with total growth extent, $w \ll l$ (section S1 shows the CNT length required for successful chirality selection at a given reaction zone width, w). The outcome of such a cycle of growth followed by a reversed dissolution will be a well-preserved single-chirality CNT of the arbitrarily chosen type.

DISCUSSION

Such near-equilibrium forward-back kinetics may be slow, while practical faster reactions occur not close enough to equilibrium to fully obey the detailed balance. Even then, for the often accepted dislocation growth mechanisms, mentioned above, growth and etching atomistic events (C additions or detachments) do occur at the kinks, so the rate constants are both proportional to the number of kinks, k_χ, $k^-_\chi \propto \chi$ (*1*, *15*), and the near-proportionality in Fig. 4A should hold.

If the reaction reversal involves appreciable reconstruction of the edge or catalyst, then the functions k^-_χ and k_χ may become not simply proportional to each other, as in Fig. 4B. If condition $k^-_\chi \propto k_\chi$ does not hold, then still some chiral types can be produced selectively by being canvassed into the white rectangle, a clear possibility for some (solid blue) but not other (red circles) chiral types. This is easy to see geometrically (Fig. 4B).

A note worth making for practical realizations is that although a localized reaction zone (for growth or dissolution) is entirely feasible by a nozzle supply of the reactants (*30*), the local temperature T can be more readily modulated. Because most of the chemical rates k, k^- are governed by Arrhenius temperature dependence $\sim e^{-E/kT}$, any

temperature distribution will modulate reactions in the same way as a much sharper concentration window would. A notable example among the most common distributions, a Lorentzian shape $T(x) = T_0/(1 + x^2)$, neglecting the much cooler background, results in a Gaussian of reaction rates akin to concentration profile $\sim G(x) = e^{-(E/kT)x^2}$; its spatial width is $\sqrt{(E/k_bT)}$ times smaller than for T.

The above shows that any desired CNT chiral type can be produced selectively by means of localized reactions, with the growth first performed at conditions where the targeted chirality is the slowest among surviving and growing, and then reversing the process from growth to recession (etching), where the desired CNTs are a notch below the slowest fully reduced, so they are all preserved again. It may be worth reiterating that the ingredients that our strategy relies on have all been achieved, with ample experimental evidence: floating catalyst "kite" growth (*25*–*28*), production of long (up to a meter) tubes (*25*–*28*), including the single wall (*28*), feedstock gas supply via a local but moving nozzle (*30*), nanotube etching (*34*), etc. There are no missing, unsupported by experimental evidence, components or principal obstacles to the proposed strategy. We realize how simplified and abstract our analysis is, at this point, intentionally omitting chemical specifics of the reactions (choice of the feedstock reactants in growth and in its reversal) or physical magnitudes of concentrations, speed, and width of the zone. Still, we believe that the clear insight gained should motivate direct laboratory experiments and further computational models, exploring details and possibilities in solving this long-standing problem of single-chirality nanotube synthesis.

MATERIALS AND METHODS

Chemical kinetics

Chemical kinetics theory (*37*), in combination with well-established methods of designation (*3*, *38*) of nanotubes chirality (helical symmetry) was used for derivations. The reaction rate is the time derivative of the extent of the reaction $(dn_i/dt)/\nu_i$, where dn_i is a change in the amount of the reaction component i, reactant, or product and ν_i is the stoichiometric coefficient of that component. In the present case, this rate is proportional to the feedstock concentration c, as $k{\cdot}c$, defining the reaction rate constant k. For convenience, in our derivations, the reaction rate of carbon attachment/detachment to CNT is replaced with the speed of CNT elongation, which is the same as the speed of catalyst particle $v = dl/dt$. This conversion does not affect any dependencies because the CNT length is proportional to the number of incorporated atoms but allows for direct comparison between the CNTs' growth speeds and the progression of the moving (at speed V) reaction zone.

Atomistic structure

The atomistic structure in the inset in Fig. 1 shows a (7,5) nanotube in contact with the Ni catalyst nanoparticle. Although it is used here as illustration only, the method to generate its fully realistic geometry relied on the interatomic forces quantified by the well-tested ReaxFF potential (*39*).

Stability analysis

The mathematical solutions, roots of Eq. 1, guiding the CNT growth (Figs. 1B and 3, A and B) are tested for stability using the standard method of classical (nonquantum) perturbation theory: A small perturbation in length δx, concentration $\delta c(x)$, or temperature $\delta T(x)$ is introduced near the stationary point, and then, its evolution in time is calculated to determine whether it is increasing or decreasing back to zero value. As a result, one root in Fig. 2 (A and B) [cf. figure 2 in (*40*)] is recognized as a Lyapunov stable and another as unstable (*41*).

Detailed balance and reciprocity

In the discussion of dissolution/etching, their rate constants k^-_χ proportionality to the corresponding k_χ of growth (i.e., k^-_χ/k_χ being the same for different χ types) is motivated by the methods of nonequilibrium thermodynamics, detailed balance principle, and the Onsager reciprocity relations (*42*, *43*). Exploring this connection in detail would take us too far afield. Furthermore, these rigorous relationships are only valid close to equilibrium. In reality, both forward (growth) and reverse (etching) speeds reach practically useful magnitudes only sufficiently far from equilibrium, where possible rearrangements of the CNT edge, catalyst-tube interface, or even catalyst phase change could become the factors coming into play. These departures from the k^-_χ/k_χ = const are already shown in Fig. 4B.

Ordinary differential equations

The section S1, by solving the ordinary differential equation $dl/dt = k{\cdot}c(l)$, evaluates the required minimum length of selected CNTs necessary for the successful single chirality production through the evolutionary selection approach given the half width of the reaction zone w and resolution of the growth speed Δk. For simplicity, the concentration profile is taken to be the Gaussian with the corresponding half-width w and peak concentration of c_o. The reaction was assumed to seize completely at concentrations below $<0.001c_o$. The growth speed of the selected CNT was taken approximately from the literature as k_sc_o = 10 μm/min (*34*). Because only scarce experimental data is available concerning the etching speed, it was assumed to be an order of magnitude slower than growth. We only explicitly consider the separation of the selected tube from the CNTs with the growth (and etching) speeds closest to that of the selected tube. The resolution of the growth speed Δk or the difference between the growth speed of the selected CNT and the closest slower- and faster-growing tubes was expressed in the percent of the selected tube growth speed and assumed to be the same in the positive and negative direction. The change of CNT lengths during growth and etching cycles (see fig. S1) was evaluated through numerical integration with Euler method (*41*, *44*) of $dl/dt = k{\cdot}c(x - Vt)$. The final results for the half-width range of w = 0.25 to 1.5 mm and growth speed resolution of Δk = 1 to 40% are shown in fig. S2.

SUPPLEMENTARY MATERIALS

Supplementary material for this article is available at https://science.org/doi/10.1126/sciadv.add4627

REFERENCES AND NOTES

1. S. Iijima, Helical microtubules of graphitic carbon. *Nature* **354**, 56–58 (1991).
2. S. Iijima, T. Ichihashi, Single-shell carbon nanotubes of 1-nm diameter. *Nature* **363**, 603–605 (1993).
3. B. I. Yakobson, R. E. Smalley, Fullerene nanotubes: $C_{1,000,000}$ and beyond. *Am. Sci.* **85**, 324–337 (1997).
4. N. Gupta, E. S. Penev, B. I. Yakobson, Fatigue in assemblies of indefatigable carbon nanotubes. *Sci. Adv.* **7**, eabj6996 (2021).
5. Y.-L. Li, I. A. Kinloch, A. H. Windle, Direct spinning of carbon nanotube fibers from chemical vapor deposition synthesis. *Science* **304**, 276–278 (2004).
6. M. Davenport, Much ado about small things. *Chem. Eng. News* **93**, 10–15 (2015).

7. M. Zheng, A. Jagota, E. D. Semke, B. A. Diner, R. S. Mclean, S. R. Lustig, R. E. Richardson, N. G. Tassi, DNA-assisted dispersion and separation of carbon nanotubes. *Nat. Mater.* **2**, 338–342 (2003).
8. M. Zheng, A. Jagota, M. S. Strano, A. P. Santos, P. Barone, S. G. Chou, B. A. Diner, M. S. Dresselhaus, R. S. Mclean, G. B. Onoa, G. G. Samsonidze, E. D. Semke, M. Usrey, D. J. Walls, Structure-based carbon nanotube sorting by sequence-dependent DNA Assembly. *Science* **302**, 1545–1548 (2003).
9. M. S. Arnold, A. A. Green, J. F. Hulvat, S. I. Stupp, M. C. Hersam, Sorting carbon nanotubes by electronic structure using density differentiation. *Nat. Nanotechnol.* **1**, 60–65 (2006).
10. F. Yang, X. Wang, D. Zhang, J. Yang, D. Luo, Z. Xu, J. Wei, J.-Q. Wang, Z. Xu, F. Peng, X. Li, R. Li, Y. Li, M. Li, X. Bai, F. Ding, Y. Li, Chirality-specific growth of single-walled carbon nanotubes on solid alloy catalysts. *Nature* **510**, 522–524 (2014).
11. F. Yang, X. Wang, J. Si, X. Zhao, K. Qi, C. Jin, Z. Zhang, M. Li, D. Zhang, J. Yang, Z. Zhang, Z. Xu, L.-M. Peng, X. Bai, Y. Li, Water-assisted preparation of high-purity semiconducting (14,4) carbon nanotubes. *ACS Nano* **11**, 186–193 (2017).
12. X. Zhang, B. Graves, M. De Volder, W. Yang, T. Johnson, B. Wen, W. Su, R. Nishida, S. Xie, A. Boies, High-precision solid catalysts for investigation of carbon nanotube synthesis and structure. *Sci. Adv.* **6**, eabb6010 (2020).
13. K. Chang, "It slices! It dices! Nanotube struts its stuff," *New York Times*, 2002.
14. R. Rao, D. Liptak, T. Cherukuri, B. I. Yakobson, B. Maruyama, In situ evidence for chirality-dependent growth rates of individual carbon nanotubes. *Nat. Mater.* **11**, 213–216 (2012).
15. F. Ding, A. R. Harutyunyan, B. I. Yakobson, Dislocation theory of chirality-controlled nanotube growth. *Proc. Natl. Acad. Sci. U.S.A.* **106**, 2506–2509 (2009).
16. V. I. Artyukhov, E. S. Penev, B. I. Yakobson, Why nanotubes grow chiral. *Nat. Commun.* **5**, 4892 (2014).
17. M. J. Bronikowski, P. A. Willis, D. T. Colbert, K. A. Smith, R. E. Smalley, Gas-phase production of carbon single-walled nanotubes from carbon monoxide via the HiPco process: A parametric study. *J. Vac. Sci. Technol. A* **19**, 1800–1805 (2001).
18. M. Chhowalla, K. B. K. Teo, C. Ducati, N. L. Rupesinghe, G. A. J. Amaratunga, A. C. Ferrari, D. Roy, J. Robertson, W. I. Milne, Growth process conditions of vertically aligned carbon nanotubes using plasma enhanced chemical vapor deposition. *J. Appl. Phys.* **90**, 5308–5317 (2001).
19. P. B. Amama, C. L. Pint, L. McJilton, S. M. Kim, E. A. Stach, P. T. Murray, R. H. Hauge, B. Maruyama, Role of water in super growth of single-walled carbon nanotube carpets. *Nano Lett.* **9**, 44–49 (2009).
20. M. Bedewy, E. R. Meshot, H. Guo, E. A. Verploegen, W. Lu, A. J. Hart, Collective mechanism for the evolution and self-termination of vertically aligned carbon nanotube growth. *J. Phys. Chem. C* **113**, 20576–20582 (2009).
21. S. Huang, X. Cai, J. Liu, Growth of millimeter-long and horizontally aligned single-walled carbon nanotubes on flat substrates. *J. Am. Chem. Soc.* **125**, 5636–5637 (2003).
22. S. Huang, M. Woodson, R. Smalley, J. Liu, Growth mechanism of oriented long single walled carbon nanotubes using "fast-heating" chemical vapor deposition process. *Nano Lett.* **4**, 1025–1028 (2004).
23. L. X. Zheng, M. J. O'Connell, S. K. Doorn, X. Z. Liao, Y. H. Zhao, E. A. Akhadov, M. A. Hoffbauer, B. J. Roop, Q. X. Jia, R. C. Dye, D. E. Peterson, S. M. Huang, J. Liu, Y. T. Zhu, Ultralong single-wall carbon nanotubes. *Nat. Mater.* **3**, 673–676 (2004).
24. Z. Jin, H. Chu, J. Wang, J. Hong, W. Tan, Y. Li, Ultralow feeding gas flow guiding growth of large-scale horizontally aligned single-walled carbon nanotube arrays. *Nano Lett.* **7**, 2073–2079 (2007).
25. R. Zhang, Y. Zhang, Q. Zhang, H. Xie, W. Qian, F. Wei, Growth of half-meter long carbon nanotubes based on Schulz-Flory distribution. *ACS Nano* **7**, 6156–6161 (2013).
26. Y. Bai, H. Yue, J. Wang, B. Shen, S. Sun, S. Wang, H. Wang, X. Li, Z. Xu, R. Zhang, F. Wei, Super-durable ultralong carbon nanotubes. *Science* **369**, 1104–1106 (2020).
27. R. Zhang, Y. Zhang, F. Wei, Controlled synthesis of ultralong carbon nanotubes with perfect structures and extraordinary properties. *Acc. Chem. Res.* **50**, 179–189 (2017).
28. X. Wang, Q. Li, J. Xie, Z. Jin, J. Wang, Y. Li, K. Jiang, S. Fan, Fabrication of ultralong and electrically uniform single-walled carbon nanotubes on clean substrates. *Nano Lett.* **9**, 3137–3141 (2009).
29. A. van der Drift, Evolutionary selection, a principle governing growth orientation in vapour-deposited layers. *Philips Res. Repts* **22**, 267 (1967).
30. I. V. Vlassiouk, Y. Stehle, P. R. Pudasaini, R. R. Unocic, P. D. Rack, A. P. Baddorf, I. N. Ivanov, N. V. Lavrik, F. List, N. Gupta, K. V. Bets, B. I. Yakobson, S. N. Smirnov, Evolutionary selection growth of two-dimensional materials on polycrystalline substrates. *Nat. Mater.* **17**, 318–322 (2018).
31. V. Pimonov, H.-N. Tran, L. Monniello, S. Tahir, T. Michel, R. Podor, M. Odorico, C. Bichara, V. Jourdain, Dynamic instability of individual carbon nanotube growth revealed by in situ homodyne polarization microscopy. *Nano Lett.* **21**, 8495–8502 (2021).
32. E. S. Penev, K. V. Bets, N. Gupta, B. I. Yakobson, Transient kinetic selectivity in nanotubes growth on solid Co–W catalyst. *Nano Lett.* **18**, 5288–5293 (2018).
33. K. Jensen, W. Mickelson, W. Han, A. Zettl, Current-controlled nanotube growth and zone refinement. *Appl. Phys. Lett.* **86**, 173107 (2005).
34. B. Koyano, T. Inoue, S. Yamamoto, K. Otsuka, R. Xiang, S. Chiashi, S. Maruyama, Regrowth and catalytic etching of individual single-walled carbon nanotubes studied by isotope labeling and growth interruption. *Carbon* **155**, 635–642 (2019).
35. X. Feng, S. W. Chee, R. Sharma, K. Liu, X. Xie, Q. Li, S. Fan, K. Jiang, In situ TEM observation of the gasification and growth of carbon nanotubes using iron catalysts. *Nano Res.* **4**, 767–779 (2011).
36. T. Ma, W. Ren, X. Zhang, Z. Liu, Y. Gao, L.-C. Yin, X.-L. Ma, F. Ding, H.-M. Cheng, Edge-controlled growth and kinetics of single-crystal graphene domains by chemical vapor deposition. *Proc. Natl. Acad. Sci. U.S.A.* **110**, 20386–20391 (2013).
37. K. J. Laidler, *Chemical kinetics* (Prentice Hall, ed. 3, 1987).
38. G. Dresselhaus, M. S. Dresselhaus, R. Saito, *Physical Properties of Carbon Nanotubes* (World Scientific,1998).
39. J. E. Mueller, A. C. Van Duin, W. A. Goddard III, Development and validation of ReaxFF reactive force field for hydrocarbon chemistry catalyzed by nickel. *J. Phys. Chem. C* **114**, 4939–4949 (2010).
40. B. I. Yakobson, Morphology and rate of fracture in chemical decomposition of solids. *Phys. Rev. Lett.* **67**, 1590–1593 (1991).
41. V. I. Arnold, *Ordinary Differential Equations* (MIT Press, 1978).
42. F. Reif, *Fundamentals of Statistical and Thermal Physics* (McGraw-Hill, 1965).
43. L. D. Landau, E. M. Lifshitz, *Statistical Physics, Course of Theoretical Physics* (Butterworth-Heinemann, 1980) vol. 5.
44. K. A. Atkinson, *An Introduction to Numerical Analysis* (John Wiley & Sons, ed. 2, 1989).
45. D. Hagen, J. J. Beaman, D. Kovar, Selective laser flash sintering of 8-YSZ. *J. Am. Ceram. Soc.* **103**, 800–808 (2020).

Acknowledgments

Funding: This work was supported by National Science Foundation (NSF) grant number CBET-1605848 and, in part, by the Robert Welch Foundation (C-1590). **Author contributions:** B.I.Y. conceived of the project. K.V.B. performed computations. Both wrote the manuscript. **Competing interests:** The authors declare that they have no competing interests. **Data and materials availability:** All data needed to evaluate the conclusions in the paper are present in the paper and/or the Supplementary Materials.

Submitted 13 June 2022
Accepted 21 September 2022
Published 9 November 2022
10.1126/sciadv.add4627